

# Mapping Mangrove Using a Red-Edge Mangrove Index (REMI) Based on Sentinel-2 Multispectral Images

Zhaojun Chen, Meng Zhang<sup>D</sup>, Huaiqing Zhang, and Yang Liu

**Abstract**—Mangrove forests are among the most productive of coastal ecosystems, providing a variety of ecological functions and economic value to coastal areas around the world. Accurate identification of mangrove is of great importance for the restoration and conservation of mangrove ecosystems and for promoting the development of a blue carbon economy and achieving carbon-neutral strategies. In this study, a red-edge mangrove index (REMI) was proposed based on Sentinel-2 multispectral images, using red, green, red edge, and SWIR1 bands in the form of a (red edge-red)/(SWIR1-green) combination to highlight the unique green and moisture information of mangrove. Then, the REMI index was combined with the Otsu threshold segmentation algorithm (Otsu) to map the mangrove information with respect to Hainan Island, which has the most abundant mangrove species in China. The results indicate that, when compared with other vegetation indices, such as the normalized difference vegetation index (NDVI), enhanced vegetation index (EVI), mangrove index (MI), normalized difference MI (NDMI), combined mangrove recognition index (CMRI), and mangrove vegetation index (MVI), the REMI showed greater proficiency in distinguishing mangrove from other vegetation. When the REMI was applied to mangrove mapping in Hainan Island, the overall accuracy (OA) and kappa coefficient were 95.68% and 0.92, respectively. In addition, the mangrove distribution ranges mapped in this study were compared with existing mangrove products [HGMF\_2020 and China National Standard GB/T 7714-2015 (note)], and it was demonstrated that the mangrove distribution ranges identified based on the REMI had high coincidence with the above-mentioned mangrove products. This proves that the REMI has good potential for application in mangrove identification and mapping.

**Index Terms**—Hainan island, mangrove, red-edge mangrove index (REMI), Sentinel-2, vegetation index.

## I. INTRODUCTION

MANGROVE are communities of evergreen trees or shrubs that grow in shallow intertidal and coastal estuarine areas of tropical and subtropical coasts [1], [2], and these

Manuscript received 13 July 2023; revised 10 September 2023; accepted 6 October 2023. Date of publication 13 October 2023; date of current version 23 October 2023. This work was supported in part by the National Natural Science Foundation of China 41901385, in part by the Natural Science Foundation of Hunan Province of China 2022JJ40873, and in part by the Education Department of Hunan Province of China 21A0177. (*Corresponding author: Meng Zhang*.)

Zhaojun Chen and Meng Zhang are with the College of Forestry, Central South University of Forestry and Technology, Changsha 410004, China (e-mail: 20221200095@csuft.edu.cn; mengzhang@csuft.edu.cn).

Huaiqing Zhang and Yang Liu are with the Research Institute of Forest Resources Information Techniques, Chinese Academy of Forestry, Beijing 100091, China (e-mail: zhang@ifrit.ac.cn; liuyang@ifrit.ac.cn).

Digital Object Identifier 10.1109/TGRS.2023.3323741

communities comprise some of the most productive ecosystems on Earth [3], providing a variety of ecosystem services to coastal areas worldwide [4], [5], [6]. A mangrove ecosystem is not only a “coastal guardian” for purifying seawater, preventing wind and waves, and maintaining biodiversity, but is also one of the essential components of the blue carbon ecosystem. Studies have shown that the carbon fixation rate of mangrove is 226 g/(m<sup>2</sup>·a), which is impressive when compared with other vegetation types. Although China’s mangrove area accounts for less than two-thousandths of the global mangrove area, mangrove species account for more than one-third of the total number of species worldwide. In recent years, increasing reclamation activities, pond-farming, and indiscriminate deforestation have resulted in a drastic decrease in the mangrove forested area in China [7], [8], [9]. Although China has promulgated policies and plans related to mangrove conservation and restoration [10], [11], the mangrove ecosystem in China is facing serious challenges due to frequent human activity [12], [13] and the impact of global climate change [14]. In the face of the current trend of globalization, the construction of a rapid and high-precision automatic mangrove information extraction method is conducive to the monitoring and protection of mangrove resources, as well as to the restoration of mangrove ecosystems to mitigate global climate change. It is also of great significance in promoting the development of the blue carbon economy and achieving carbon-neutral strategies.

Remote sensing technology for monitoring mangrove has the advantages of a wide range, fast information acquisition, less restriction due to ground conditions, and nondestructivity in respect of monitoring objects [14], [15], [16], which can effectively solve the difficulties associated with mangrove research, such as the difficulty in depth and treading, and has become the main way to monitor mangrove [17], [18]. Optical and radar remote sensing data are the two main sources for mangrove mapping and dynamic changes. In previous studies relating to mangrove information identification, low–medium resolution remote sensing data sources such as NOAA/AVHRR, MODIS, Landsat MSS/TM/ETM + /OLI [19], and SPOT HRV/HRG [20], [21] were mainly utilized. With the continuous advancement of remote sensing technology and increasing image resolution, the introduction of high-resolution multispectral sensors (Sentinel-2, IKONOS, QuickBird, and Worldview) and hyperspectral sensors (ASIA+, CASI, and EO-1 Hyperion) has further enriched the data sources for mangrove monitoring [22], [23], [24].

Radar data have gradually become one of the essential data sources in mangrove monitoring due to their strong penetration and weather-independent characteristics [25] (ALOS, JERS-1, ENVISAT ASAR, Radarsat-1 SAR, and Sentinel-1A SAR), and mangrove remote sensing monitoring has gradually developed in depth. Despite different advantages of different remote sensing images, considering the spatial resolution, revisit period, coverage, and information richness of the data, Sentinel-2 data are the optimal data source for wide-scale mangrove monitoring.

In recent years, algorithms such as random forest (RF) [21], [26] support vector machine (SVM) [27], [28], and deep learning (DL) [29] have played an influential role in mangrove information acquisition. However, these algorithms require high quality of the selected sample data and the sample dataset needs to be large enough; thus, they are not suitable for fast identification of mangrove areas over a large area. Currently, the application of vegetation indices combined with the threshold method has an important status in mangrove mapping. Vegetation indices are based on vegetation spectral characteristics and combine different bands and can successfully present vegetation information and suppress nonvegetation information. Thus, vegetation indices have been widely adopted in vegetation identification and monitoring research. Numerous vegetation indices are widely employed in mangrove mapping, such as the normalized difference vegetation index (NDVI), enhanced vegetation index (EVI) [30], and ratio vegetation index (RVI) [31], [32]. However, the majority of these vegetation indices are not designed based on the characteristics of mangrove and cannot adequately distinguish mangrove from other vegetation. Consequently, some studies have focused on mangrove index (MI) construction and mangrove mapping methods, such as the MI, mangrove recognition index (MRI), NDMI, combined MRI (CMRI), mangrove forest index (MFI), and mangrove vegetation index (MVI). Although these mangrove indices have achieved better results in some study areas, unfortunately, the currently developed mangrove indices have some limitations in terms of their actual application. The MI utilizes a combination of near-infrared (NIR) and short-wave infrared (SWIR) from Landsat-8 data in conjunction with NDVI imagery to detect mangrove degradation [33]; a higher value indicates a healthier mangrove. A combination of three spectral metrics, i.e., the spectral match degree (SMD), NDMI, and short-wave infrared absorption depth (SIAD), has also been proposed to enhance the differentiation of mangrove from other vegetation [34]. However, mangrove identification using the MI and NDMI requires further testing. For some of the mangrove indices, tidal data need to be obtained, which increases the uncertainty in the accuracy of mangrove extraction. For example, the MRI selects the vegetation greenness index and moisture index to effectively express the complex characteristics of mangrove habitats [35]. Due to different tidal conditions and the diversity of vegetation in each region, specific tidal information and vegetation information are required in mangrove identification. Partial mangrove vegetation indices are not suitable for large-area mapping due to the large sample size. For instance, compared with the MRI, the CMRI can further amplify the

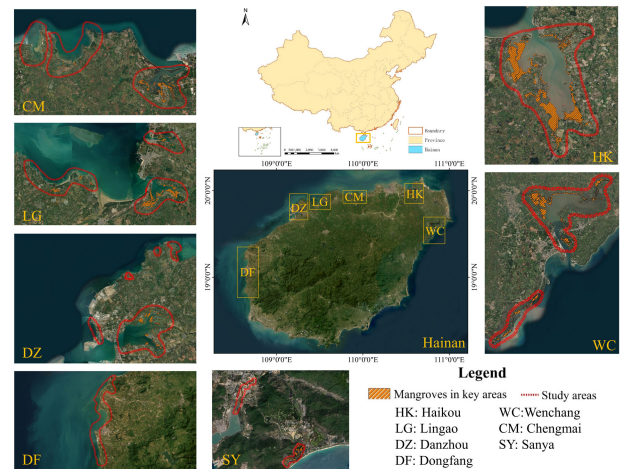


Fig. 1. Location of the study area.

spectral feature information of mangrove similarity to other vegetation through the negative correlation between the NDVI and normalized difference water index (NDWI), and then, the CMRI can be used as a feature variable for the input of classification methods [36]. However, the CMRI index-based approach requires substantial training data to generate mangrove maps. In addition, Jia et al. [37] developed an MFI utilizing the principle that submerged vegetation has a strong reflection in the red-edge band. The results demonstrated that the index can distinguish the inundated mangroves from the water background well. However, the applicability of the index to nonsubmerged mangrove vegetation needs to be further explored. As a result, the construction of a stable and widely applicable MI based on the spectral characteristics of mangrove is a key issue to be solved for mangrove mapping and monitoring.

Inspired by these mangrove indices, we propose a red-edge mangrove index (REMI) for mapping stable mangrove distribution in this study. The proposed REMI index is intended to achieve the following objectives: 1) amplify the subtle differences between mangrove and other vegetation; 2) avoid dealing with large sample datasets; and 3) obtain stable mangrove classification results. The MI developed in this study was created by combining and calculating different bands based on the characteristics of mangrove, providing scientific support for mangrove monitoring and protection.

## II. STUDY AREA AND DATA SOURCES

### A. Study Area

Hainan Island is located at approximately  $18^{\circ}10' \text{--} 20^{\circ}10'$   $108^{\circ}37' \text{--} 111^{\circ}03'$  N latitude. It is on the edge of the tropics and has a tropical maritime monsoon climate with an average annual temperature of  $22.5^{\circ}\text{C}$ – $25.6^{\circ}\text{C}$  and annual precipitation of 1500–2500 mm. The positive rain and heat conditions are conducive to the growth of mangrove (Fig. 1). Hainan Island has the richest mangrove species in China (26 species of true mangrove plants) [19], one national mangrove nature reserve, and two provincial mangrove nature reserves, which are crucial to the ecological, economic, and sustainable development of Hainan Province. The topography

of Hainan Island is high in the middle and low elsewhere. The rivers are radially distributed, providing favorable terrain for the growth of mangrove. The coastal harbors and river mouths are the important growth areas of mangrove and are mainly concentrated in Dongzhai Port National Nature Reserve, Qinglan Port Provincial Nature Reserve, the southeast area (i.e., Sanya), the northwest area (Lingao, Chengmai, and Danzhou), and the southwest area (i.e., Dongfang) of Hainan Island.

### B. Data Source

*1) Sentinel-2 Imagery:* Sentinel-2 is a high-resolution multispectral satellite that includes two simultaneously operating polar satellites (Sentinel-2A, launched in 2015, and Sentinel-2B, launched in 2017), of which the two satellites combined have a short revisit period (5 days) and make it easier to obtain cloud-free images. The Sentinel-2 satellite carries a multispectral imager (MSI) that covers up to 13 spectral bands and is the only satellite that contains information in three red-edge bands; this is vital for identifying and monitoring vegetation. We acquired 2020 Sentinel-2 level-2A data, which contains surface reflectance data based on the GEE cloud platform. The obtained Sentinel-2 images had been orthorectified and did not require further processing such as radiometric calibration and atmospheric correction. In order to avoid the uncertainty resulting from tidal inundation in the interpretation of mangrove mapping, images at low tide (tide height below 0.5 m) were selected as much as possible according to tidal information provided by the China Maritime Services Network (<https://www.cnss.com.cn/html/tide.html>) and Global Tide Forecasting Platform (<http://global-tide.nmdis.org.cn/>). As a result of screening, a total of 18 views of 2020 Sentinel-2 cloud-free images were downloaded for this study.

*2) Field Survey Data:* The field survey was focused on the period March–May 2020, which was primarily used for subsequent mangrove mapping accuracy verification. The mangrove forest and other vegetation in the neighboring areas were surveyed by means of Office of War Information (OWI) map positioning pointing, field photography, and measurement [real-time kinematic (RTK)]. The information recorded mainly included sample point location, vegetation types, photography, and the growth of mangrove forests. In addition, we generated more mangrove sample datasets (Fig. 2) by referring to existing mangrove distribution products (e.g., the HGMF\_2020 dataset), ensuring that the number of mangrove sample points was approximately double that of other vegetation sample points.

*3) Mangrove Products:* The mangrove growth environment is complex and mainly distributed in the mudflat area, which is difficult to investigate in depth in the field. Therefore, the following two mangrove products were applied to determine the core distribution area of mangrove forests on Hainan Island (Fig. 1) and assisted in generating a mangrove validation sample set for this study.

*a) HGMF\_2020 dataset:* The dataset was sourced from the International Research Center of Big Data for Sustainable Development Goals (SDG Center) and was produced by Jia et al. [38] (<http://www.cbas.ac.cn/>). The dataset was generated by combining the maximum value synthesis algorithm

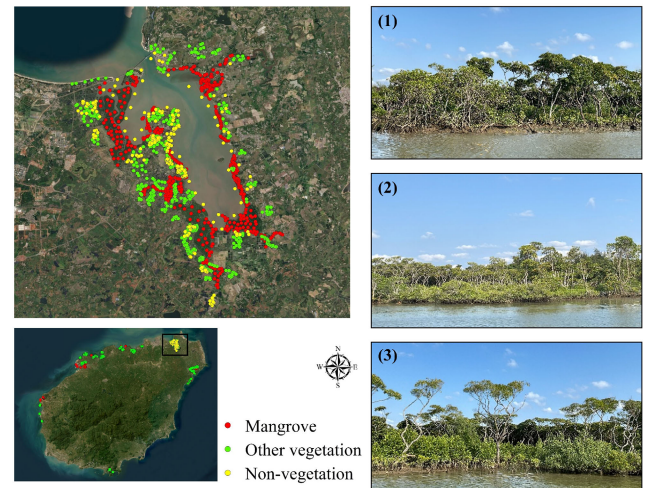


Fig. 2. Spatial distribution of field survey sample points (where (1)–(3) are the mangrove field survey photographs).

(MSIC) and object-oriented RF algorithm (OBRF) through remote sensing big data and the GEE cloud platform to map the first global mangrove distribution dataset with high spatial resolution (10 m) and overall mapping accuracy of over 95%. The HGMF\_2020 dataset fully considers the tidal influence, and the spatial coverage and boundaries of mangrove patches are clearly mapped.

*b) China National Standard GB/T 7714-2015 (note):* The dataset was produced by mapping the spatial distribution of mangrove in Hainan Island from 2015 to 2019 based on domestically produced Gaofen-2 (GF-2) data, with an overall mapping accuracy of 99%, using an SVM algorithm [39].

*4) Auxiliary Data:* The auxiliary data include Google Earth Engine high-resolution images, TidalChina\_1995-2015, and the 2020 global land use and land cover ESRI dataset (10 m), which were mainly utilized to distinguish land use types and determine the extent of mangrove. TidalChina\_1995-2015 is an intertidal dataset that was obtained by integrating remote sensing and geographic information system (GIS) methods based on 156 views of Landsat TM/OLI satellite images covering the national coastal area in 1995 and 2015 (<https://www.geodoi.ac.cn/>). The ESRI dataset was derived from ESA Sentinel-2 imagery and mapped using a deep-learning model with an overall accuracy (OA) of 85% (<https://code.earthengine.google.com/>). We also utilized vector data, topographic data [digital elevation model (DEM)], and tidal data of Hainan Province for assisting with mangrove identification and mapping, where topographic data were from the Geospatial Data Cloud (<https://www.gscloud.cn/>), and tidal data were from the Global Tide Forecasting Platform (<http://global-tide.nmdis.org.cn/>) and the China Maritime Services Network (<https://www.cnss.com.cn/html/tide.html>).

## III. METHODOLOGY

### A. Development of REMI

*1) Band Selection for REMI Construction:* We randomly and uniformly selected 500 training sample points each for mangrove and other vegetation types, which were used to analyze the reflectance of features in the study area. Based on

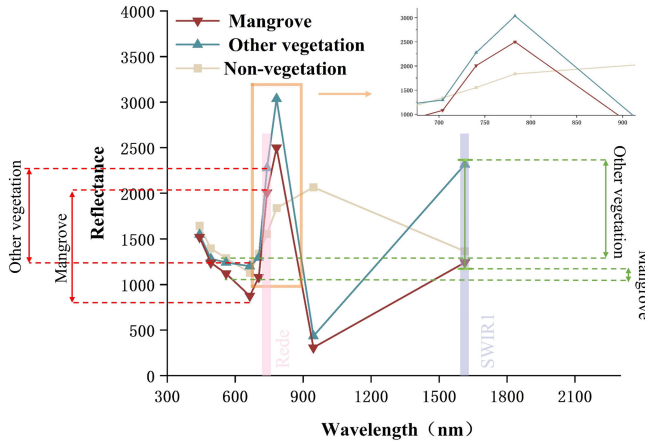


Fig. 3. Spectral characteristic curves based on mangrove, other vegetation, and nonvegetation.

the spectral characteristic curves of each species (Fig. 3), it can be observed that the reflectance values of mangrove in the red-edge band and SWIR1 band are significantly different from other vegetation, and it has been demonstrated that the red-edge band and SWIR1 band can successfully express the unique greenness and moisture information of mangrove [38]. In the reflectance curve, the reflectance increased rapidly near the red-edge band (700–800 nm), and the difference between mangrove and other vegetation in this spectral region was obvious. Therefore, the spectral characteristics of the red-edge region are important for vegetation classification, health condition monitoring, and biological parameter estimation [40], [41]. While SWIR1 and SWIR2 both express the effects of tidal inundation on mangrove [42], SWIR1 is more effective in identifying vegetation [43]. Mangrove are subject to periodic inundation by seawater, and the high-salt growth environment promotes water uptake by mangrove roots, so the process of information extraction from mangrove is bound to be influenced by the soil and moisture background. The difference in reflectance between mangrove and other vegetation is more obvious in the SWIR1 band, which can magnify the difference between mangrove and other vegetation better. In addition, in the visible range, the spectral characteristic curve of green vegetation shows a typical “green peak” and “red valley” variation [44], [45] mainly due to the strong reflection of green light and strong absorption of red light by chlorophyll. Therefore, four multispectral band combinations are proposed to express the mangrove vegetation information: red (band 4), green (band 3), red edge (band 5/6/7), and SWIR1 (band 11).

2) *Formulation of REMI:* Both mangrove and other vegetation have higher reflectance values in the red-edge and SWIR wavelengths than in the visible range. In general, the reflectance of the red-edge region depends on the internal chlorophyll content, and the “blue shift” and “red shift” of the red-edge position will occur with the change in chlorophyll content [46], [47]. Due to the strong absorption of chlorophyll in the red-light band, the sensitivity of the vegetation index to chlorophyll content is reduced, while chlorophyll absorption is reduced in the red-light border region, which in turn effectively

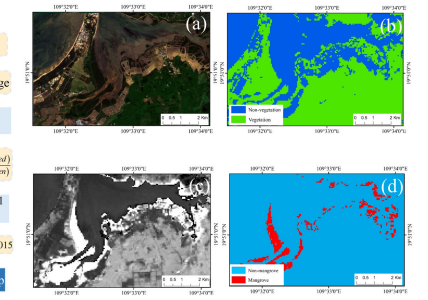


Fig. 4. General structure of the research method. (a) NDVI maximum composite image, (b) vegetation coverage, (c) REMI maximum composite image, and (d) initial coverage of mangrove.

reduces the impact of the chlorophyll saturation effect. In the other vegetation samples, when the reflectance values of other vegetation in the red-edge band are higher, lower values of red reflectance can be found instead, but none of them are lower than the red reflectance values of mangrove. Other vegetation with high reflectance in the red-edge band will also have higher values in the SWIR1 band than mangrove and will have relatively higher green values. The difference between mangrove and other vegetation will be larger if the red-light reflectance value is subtracted from the red-edge band, and smaller if the green-light reflectance value is subtracted from the SWIR1 reflectance value.

The REMI equation is as follows:

$$REMI = \frac{(red\ edge - red)}{(SWIR1 - green)} \quad (1)$$

where red edge, red, SWIR1, and green are the reflectance values of the 6th, 4th, 11th, and 3rd bands of Sentinel-2, respectively. The upper part of the equation (red edge and red) enhances the difference in greenness between mangrove and other vegetation, and the lower part of the equation (SWIR1—green) highlights the information on the moisture contained in mangrove due to the growing environment. The REMI emphasizes the unique greenness and moisture of mangrove through red light, green light, red edge, and SWIR1 to amplify the differences between mangrove and other vegetation. In this study, the REMI was normalized to between −1 and 1. Usually, the REMI value is positive and the larger quotient value indicates that the pixel has a higher probability of being a mangrove.

#### B. Mangrove Information Extraction by Combining REMI and Otsu Algorithm

In this article, we propose an automatic mangrove classification method based on the REMI and the Otsu algorithm [1], [24], and the specific implementation technology route is shown in Fig. 4. First, high-quality Sentinel-2 image sets were obtained by preprocessing to analyze the spectral response of mangrove, other vegetation, and nonvegetation. Subsequently, NDVI maximum and REMI maximum images were generated and then combined with the Otsu algorithm to derive the mangrove growth range. Finally, the accuracy of the mangrove extraction results was verified using validation sample sets

such as field survey data. Mangrove mapping based on the REMI with Otsu consists of two parts.

- 1) the NDVI is selected to synthesize the NDVI maximum image, and the minimum water surface image (i.e., the water surface at low tide) [48] is then generated. Next, the Otsu algorithm is used to segment the “minimum water surface image” by selecting the NDVI threshold. If the NDVI value is greater than or equal to 0.5, the pixel is vegetation, otherwise it is not vegetation.
- 2) Combining REMI maximum synthetic images with the vegetation coverage (mangrove and other vegetation), using the Otsu algorithm, and determining the optimal REMI threshold, the final automatic classification of mangrove and other vegetation is accomplished.

As mangrove REMI values are higher than those of other vegetation, the initial range of mangrove was first chosen in this study. However, there would still be cases where false pixels were categorized as mangrove in the initial range of mangrove obtained, such as areas far from coastal ports and not affected by tides. Therefore, we utilized the intertidal zone provided by TidalChina\_1995–2015 to further delineate the initial extent of mangrove. Since the errors associated with the application of the TidalChina\_1995–2015 intertidal zone in small areas may be large [49], we used visual interpretation combined with Sentinel-2 imagery in small areas to manually adjust the extent of the intertidal zone to minimize errors and improve the accuracy of mangrove extraction.

Due to the uneven distribution and complex composition of mangrove in Hainan Island, it is difficult to obtain a uniform threshold value. In order to accurately extract mangrove, we conducted several experiments to count the threshold values in different areas. Although the REMI threshold varies from region to region, the normalized range was roughly between 0.45 and 0.6. For large-scale mangrove mapping, the total area can be divided into several small areas based on regional conditions (mangrove type, temperature, and precipitation), and after multiple experiments, different thresholds were selected for different small areas.

### C. Mangrove Mapping Accuracy Assessment

The validation sample dataset for this article was generated with the aid of field survey data and mangrove product datasets. We compared and overlaid the two mangrove products [HGMF\_2020 and China National Standard GB/T 7714-2015 (note)] for analysis, and then, the overlap between the two was used as a candidate for the validation sample set. In this study, the accuracy assessment included both mangrove and nonmangrove species. The mangrove classification accuracy evaluation was performed based on the validation dataset using the confusion matrix, and the assessment metrics included user accuracy (UA), producer accuracy (PA), OA, and kappa coefficient.

## IV. RESULTS AND ANALYSIS

### A. Comparison of REMI With Other Remote Sensing Indices

In this study, two common vegetation indices (NDVI and EVI) and one water body index (NDWI) were selected

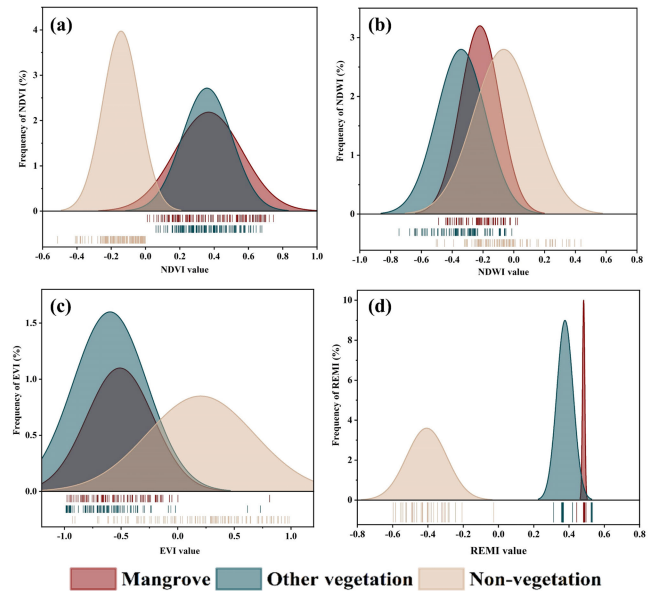


Fig. 5. Histograms of different indices. (a) NDVI, (b) NDWI, (c) EVI, and (d) REMI.

to analyze their ability to distinguish mangrove from other vegetation and to compare them with the REMI constructed in this research. Four indices were calculated by randomly and uniformly selecting mangrove, other vegetation, and nonvegetation sample points, after which normal distribution plots were generated for each index (Fig. 5). The results indicate that NDVI, EVI, and NDWI could not accurately distinguish mangrove from other vegetation. Most of these commonly used remote sensing indices consist of a combination of visible and NIR reflectance, with the most common combination being a “red absorption peak” and “NIR” bands. However, the reflectance of the “red absorption peak” tends to saturate in areas with high vegetation cover, which makes it less sensitive to vegetation and makes it difficult to distinguish mangrove from other vegetation in areas with high cover. Compared with other indices, the red-edge band was chosen and combined with the red-light band in the REMI, which addressed the problem of red-light band reflectance saturation while also highlighting the greenness information, resulting in better distinction between mangrove and other vegetation. High REMI values indicate healthier mangrove vegetation (higher red-edge reflectance) that contains more chlorophyll (higher greenness), while higher REMI values also indicate greater water uptake.

In this study, we compared the capabilities of the REMI, CMRI, NDMI, MVI, MI, and common indices (NDVI, EVI, and NDWI) to distinguish mangrove from other vegetation on a quantitative basis. We randomly and uniformly selected 300 sample points for mangrove, other vegetation, and non-vegetation, and calculated the values of each of the six indices. As shown in Fig. 6, the NDVI and EVI are vegetation indices, and the CMRI is a combination of the NDVI and NDWI, so all three vegetation indices perform well in their ability to distinguish vegetation from nonvegetation. According to the characteristics of the median of the boxplot, it is obvious

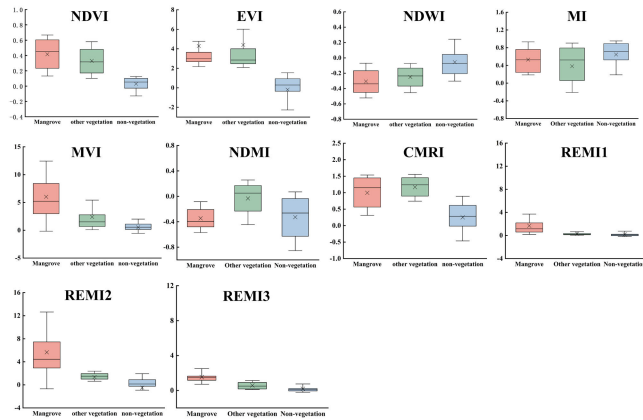


Fig. 6. Boxplot of ten indices based on Sentinel-2 images for three land cover types. (REMI1, REMI2, and REMI3 are based on red-edge bands 5–7, respectively.)

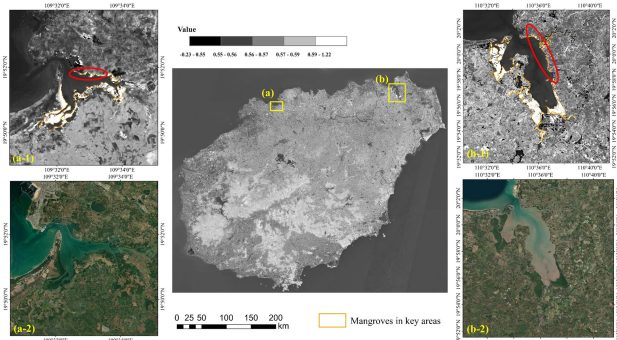


Fig. 7. Comparison of Sentinel-2-based and REMI grayscale images. (a) Dongzhai Port and (b) Xinying Port, where (a-1) and (b-1) Sentinel-2 images and (a-2) and (b-2) REMI grayscale maps.

that the NDVI was more stable in distinguishing vegetation from nonvegetation than the other two indices, which is the reason why the NDVI was chosen to identify the vegetation extent in the process of mangrove information identification in this study. For mangrove and other vegetation, compared with the CMRI, MI, and NDMI, the REMI and MVI have a good ability to distinguish between them. However, the NDVI, EVI, and NDWI have difficulty in distinguishing between mangrove and other vegetation. Although mangrove have a similar greenness to other vegetation, they have a higher water content compared with other vegetation due to periodic flooding. Since the MVI and REMI highlight the greenness and moisture information, they can capture the differences between mangrove and other vegetation, while the NDVI, EVI, and NDWI cannot reflect these differences. The ability of each of the three red-edge bands (bands 5–7) combined with the red-light band in mangrove identification was analyzed. The results demonstrate that for red-edge band 6, the REMI constructed based on red-edge band 5 and red-edge band 7 had a weaker ability to distinguish mangrove from other vegetation.

In order to visualize the performance of the REMI index in distinguishing mangrove from other vegetation, Fig. 7 shows the images corresponding to the Sentinel-2 and REMI maxima in 2020. As shown by the visual interpretation, the area of high

REMI values is highly consistent with the coverage of mangrove in the HGFM\_2020 dataset and is also very similar to the distribution of mangrove in the Sentinel-2 images. This can reduce the error rate of mangrove information identification because the REMI index can better highlight the differences between mangrove and other vegetation, while preserving mangrove information. Fig. 7(a-1) and (b-1) demonstrates that the REMI also highlights mangrove information well for small intertidal patches of mangrove.

### B. Mangrove Mapping Results Based on REMI and Otsu Algorithm

Mangrove information extraction based on the REMI and Otsu algorithm yielded good classification results with an OA of 95.68% and a kappa coefficient of 0.92. The UA and PA of mangrove were 93.68% and 91.26%, respectively. Mangrove characteristics are highlighted by the REMI index, and the information with respect to mangrove characteristics is enhanced by synthesizing the REMI maximum image, which reduces the misclassification phenomenon and improves the classification accuracy. This demonstrates the feasibility of fast and accurate mangrove identification based on the REMI and Otsu algorithm in this study, providing technical and data support for mangrove wetland monitoring and management. In the study method, when extracting mangrove, there is uncertainty due to the absence of tidal data in some areas, and low-tide images in some areas are chosen to replace the cloud-free images in recent years. This leads to the existence of inundation in some mangrove and causes the PA to be lower than the UA.

**Hainan Coastal Inner Harbor:** Dongzhai Port, Qinglan Port, Huachang Port, Xinying Port, Jinjin Port, and Xinying Port are the main concentrated areas of mangrove in Hainan, in which Dongzhai Port and Qinglan Port contain a larger area of mangrove, mainly because they grow in protected areas and experience less interference from humans. Owing to the uneven distribution of coastal harbors on Hainan Island and the differences in climatic factors, the distribution of mangrove on Hainan Island is uneven, showing a spatial pattern of more in the north and less in the south, with fragmented distribution in the east and west. From the northeast to the northwest of Hainan (Wenchang to Danzhou), there are many harbors and bays along the coast with large distribution areas, which are less affected by the impact of waves. In addition, the mudflats contain a lot of sediment, which can guarantee the nutrients and environmental conditions needed for the growth of mangrove; these mudflats comprise the main distribution area of mangrove in Hainan. In the western part of Hainan toward Sanya, the distributions of outer harbors and bays are mostly affected by the impact of waves, and the mud and sand components are smaller, which is not conducive to the growth of mangrove.

## V. DISCUSSION

### A. Comparison of Mangrove Classification Results With Different Mangrove Indices

An additional four mangrove indices (CMRI, NDMI, MVI, and MI) were used to map the mangrove in the same areas to

TABLE I  
ACCURACY EVALUATION OF FIVE MANGROVE INDICES

Mangrove Indices	OA	Kappa	Mangrove		Non-mangrove	
			PA	UA	PA	UA
REMI	95.68%	0.92	91.26%	93.68%	95.37%	91.62%
CMRI	86.24%	0.80	78.62%	84.50%	94.30%	89.2%
NDMI	85.00%	0.75	80.33%	76.24%	85.30%	80.63%
MVI	92.52%	0.89	87.54%	89.54%	94.87%	86.22%
MI	81.63%	0.72	72.26%	75.82%	80.23%	82.16%

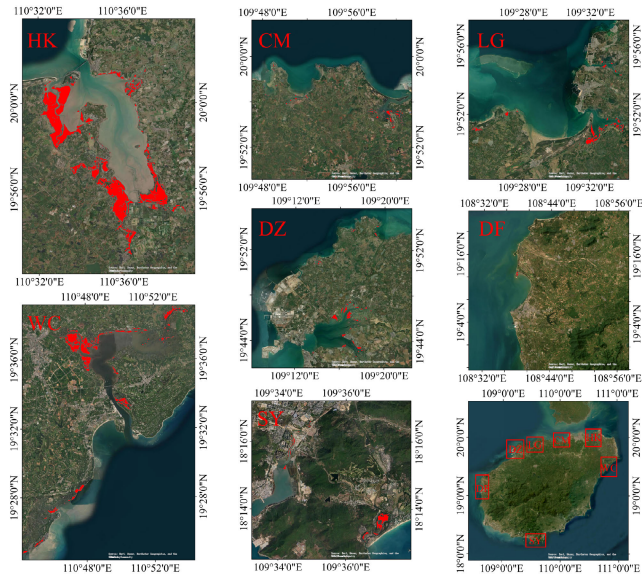


Fig. 8. Mangrove mapping results based on REMI and Otsu algorithm.

further evaluate the ability of the REMI to identify mangrove (Fig. 8). The OA and kappa coefficients of the mangrove classification results using the CMRI, NDMI, MVI, and MI were 86.24% and 0.80, 85% and 0.75, 92.52% and 0.89, and 81.63% and 0.72, respectively. The UA and PA of mangroves were 84.5% and 78.62%, 76.24% and 80.33%, 89.54% and 87.54%, and 75.82% and 72.26%, respectively. Compared with the REMI, the precision of mangrove identification results using the CMRI, NDMI, MVI, and MI were reduced, with the MI having the lowest accuracy. The UA of the CMRI index was greater than the PA, which is the reason why the CMRI index often overestimated mangrove area. In contrast, the mangrove PA of the MVI index was lower than the UA because of the obvious omission of scores. Since the MI index is used in combination with NDVI images to determine whether there is degradation of mangrove forests in a certain area, the use of the MI index alone is less generalizable for mangrove identification, resulting in poorer values of both PA and UA for mangrove forests than several other mangrove forest indices (Table I).

Mangrove maps of the same area using the CMRI, NDMI, MVI, and MI are shown in Figs. 9–12, respectively. When comparing the mangrove identification result maps of the four mangrove indices, it was found that the MI index was weak in distinguishing between mangroves and other vegetation. The MVI index was strongly influenced by the tides of the harbor, and many mangrove pixels were missed and could not be distinguished. In Dongzhai Harbor (Haikou) and

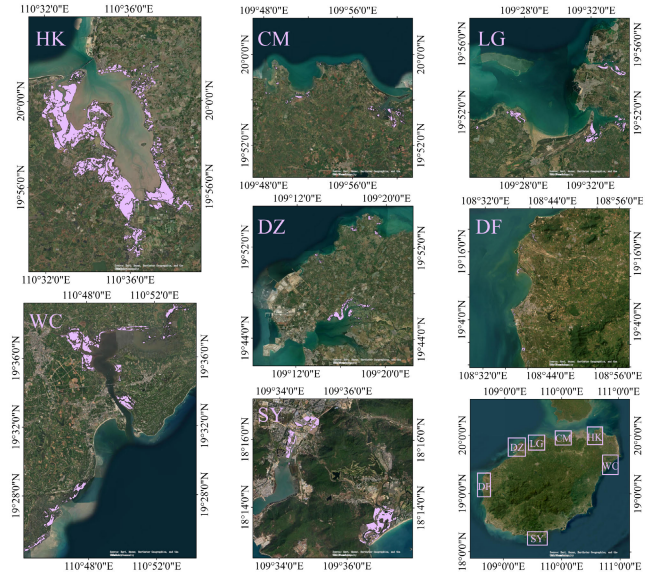


Fig. 9. CMRI-based mangrove mapping (2020).

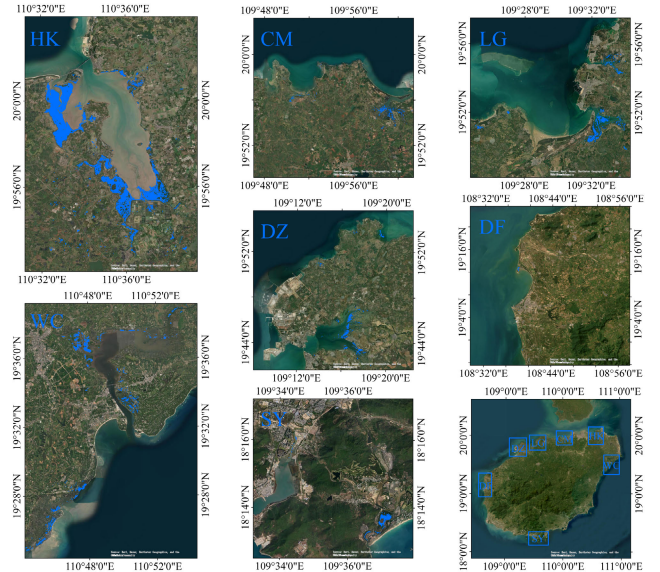


Fig. 10. NDMI-based mangrove mapping (2020).

Qinglan Harbor (Wenchang), due to the negative correlation between the NDVI and NDWI, the CMRI was prone to misclassifying phytoplankton or other aquatic plant pixels as mangroves, and thus, the mangrove area was usually overestimated. MVI-based classification results were relatively more conservative, and small mangrove pixels were missed. Compared with the CMRI, NDMI, MVI, and MI, the REMI was more capable of capturing mangrove features and identifying them accurately.

To further evaluate the ability of the five mangrove indices to distinguish mangrove from other vegetation, three small areas were selected for illustration (Fig. 13) and combined with high-resolution images for visual discrimination. It was observed that the REMI had clearer mangrove growth boundaries than the other two mangrove indices. Comparison of the mangrove distribution map with Sentinel-2 images showed that the CMRI and NDMI could not correctly distinguish mangrove from other vegetation for small mangrove areas and were

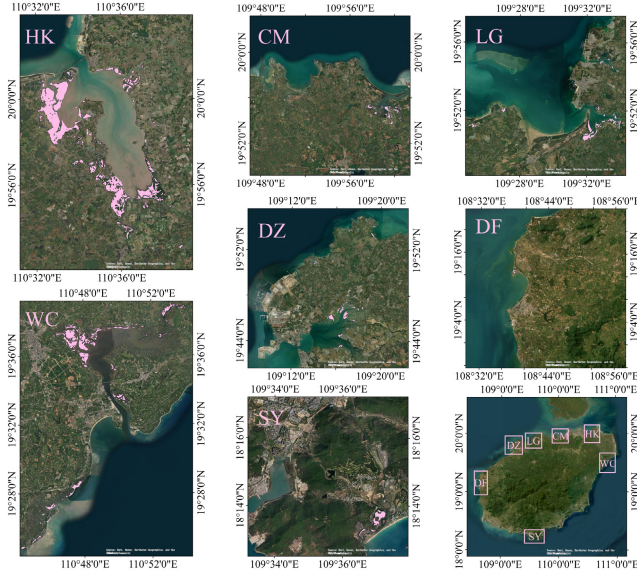


Fig. 11. MVI-based mangrove mapping (2020).

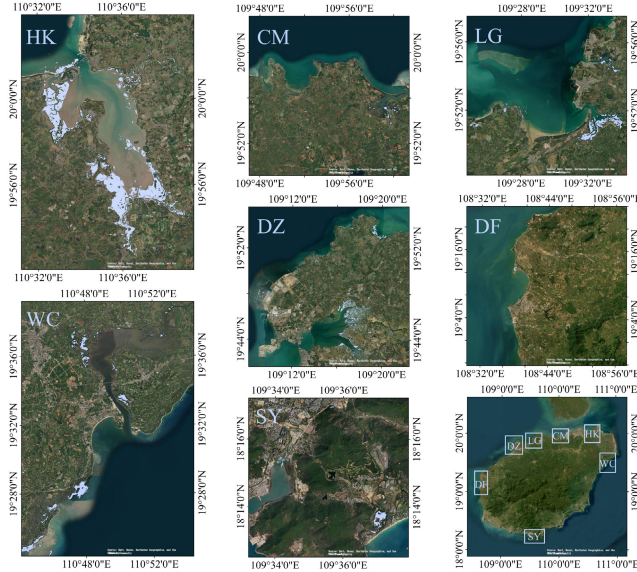


Fig. 12. MI-based mangrove mapping (2020).

prone to misclassifying other vegetation pixels as mangrove. Compared with the CMRI, the MVI and MI could correctly distinguish mangrove from other vegetation in small areas, but the classification results obtained by these indices had many mangrove omissions. In general, the mangrove classification results obtained using the REMI index had clearer boundaries, less misclassification, and less underclassification than those of the other two mangrove indices.

#### B. Comparison With Mangrove Products

A comparison of the mangrove mapping results using the REMI (Fig. 8) with the HGMF\_2020 and China National Standard GB/T 7714-2015 (note) mangrove products (Figs. 14 and 15) revealed that the REMI-based mangrove classification results were highly consistent with the above-mentioned mangrove products. This further demonstrates the feasibility of the method of mangrove identification in this study. Nevertheless, there were some differences

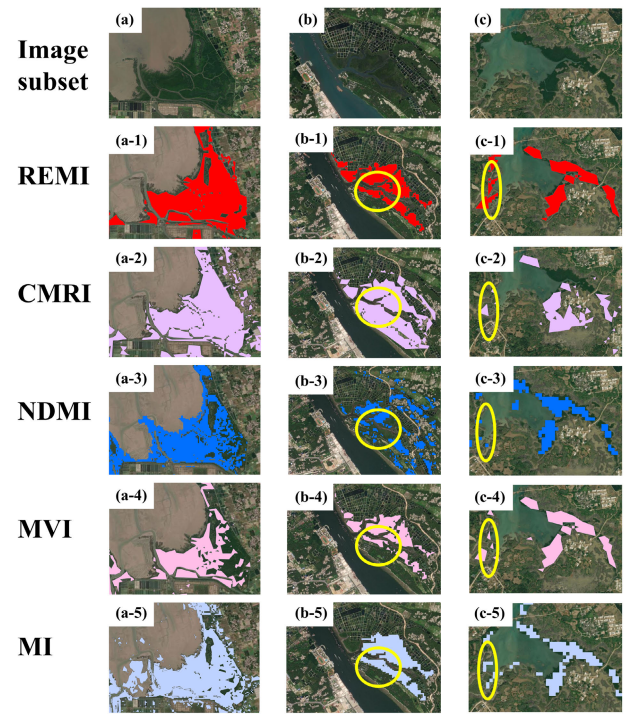


Fig. 13. Comparison of the results of mangrove information extraction using the five selected index pairs of REMI, CMRI, NDMI, MVI, and MI. Sentinel-2 remote sensing images of typical subareas, (a-1)–(c-1) are the mangrove mapping results based on REMI index, (a-2)–(c-2) are the mangrove mapping results based on CMRI index, (a-3)–(c-3) are the mangrove mapping results based on NDMI index, (a-4)–(c-4) are the mangrove mapping results based on MVI index, and (a-5)–(c-5) are the mangrove mapping results based on MI index.

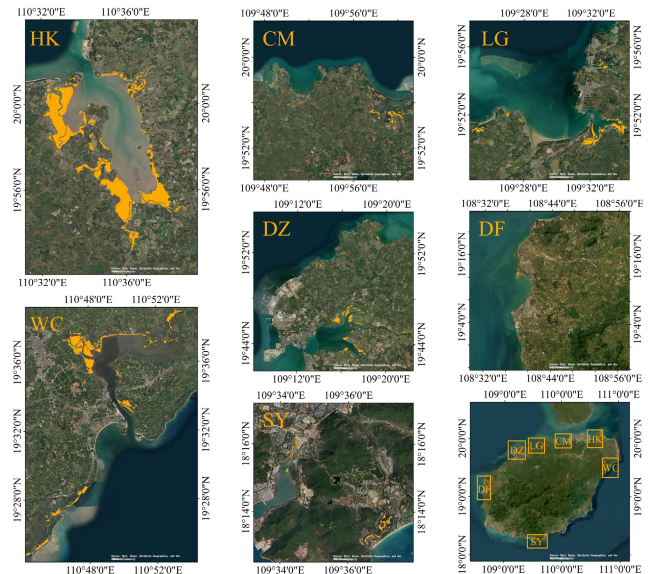


Fig. 14. HGMF\_2020.

between the mangrove distribution results obtained in this study using the REMI and Ostu and the two mangrove products (Fig. 16). Compared with the HGMF\_2020 product, the extraction results of this study showed partial mangrove omission. The remote sensing images in this article were selected during the low-tide period; however, some of the low-tide images were missing and replaced by cloudless images, which may have submerged mangrove on some of the images, thus leading to omissions in the classification of mangrove.

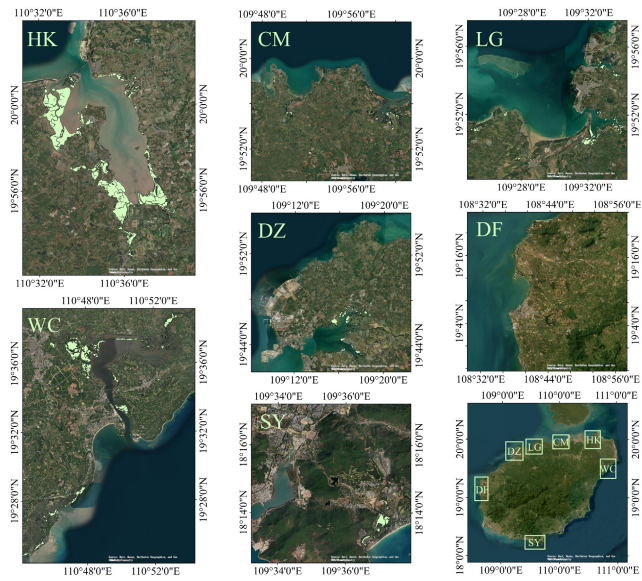


Fig. 15. China National Standard GB/T 7714-2015 (note) (2019).

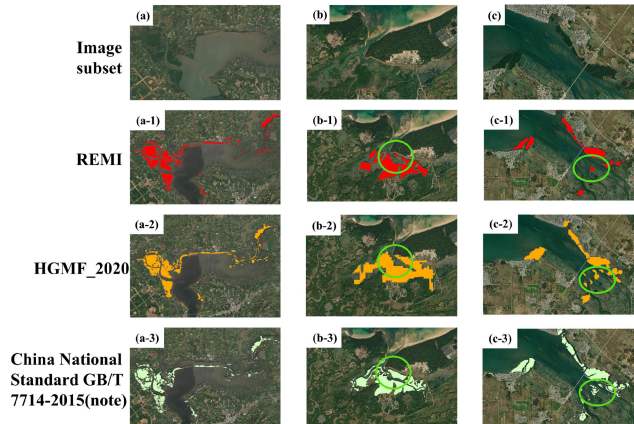


Fig. 16. Comparison of REMI and reference map. Sentinel-2 remote sensing images of typical subareas, (a-1)–(c-1) are the mangrove mapping results based on REMI index, (a-2)–(c-2) are the distribution of mangrove of HGMF\_2020 products, and (a-3)–(c-3) are the distribution of mangrove of China National Standard GB/T 7714-2015 (note) products.

Similarly, the mangrove results mapped in this article differed from the China National Standard GB/T 7714-2015 (note) dataset due to different image time period selection and spatial resolution. In this study, Sentinel-2 with high spatial resolution and rich spectral bands was adopted as the data source, and the tidal influence was taken into account to provide an accurate and fine mangrove distribution range.

#### C. Advantages and Disadvantages of REMI

In this study, a novel mangrove vegetation index REMI was developed based on Sentinel-2 MSL and applied to demonstrate its feasibility in the most abundant mangrove species region (Hainan Island) within China. The results indicate that the mangrove mapping results based on the REMI had high accuracies and had significant advantages over other mangrove indices (CMRI, NDMI, MVI, and MI). The main advantage of the REMI is reflected in the selection of the red-edge band with high sensitivity to vegetation, highlighting the greenness information with respect to mangrove, and also the selection of the red-light band to avoid the problem of

red-light saturation in densely vegetated areas and weakening sensitivity to vegetation.

Despite these advantages, the REMI index has some limitations in practical applications. Mangrove have several forms, including true mangrove plants and semimangrove plants, with true mangrove being mainly woody and similar to arboreal trees. When the REMI distinguished mangrove from other vegetation, we noticed that a small number of arboreal pixels were misclassified as mangrove. In forthcoming studies, the differences between mangrove and arboreal trees will be amplified by adding appropriate remote sensing features or new constraints to further improve the mangrove identification accuracy. The REMI is not as stable as the NDVI in distinguishing vegetation from non-vegetation, and in practical applications, it needs to be combined with the NDVI to identify the vegetation in order to map mangrove more accurately. Although cloud-free images were chosen to replace some areas, where images were missing during low-tide periods, the influence of tides on the mangrove extraction results could not be completely excluded, which is one of the important factors affecting the accuracy of classification results in this study. An attempt can be made to combine radar data with optical data during mangrove construction to compensate for the low availability of high-quality Sentinel-2 image data and low image availability to capture mangrove information.

## VI. CONCLUSION

In this study, based on the GEE platform, a novel MI was constructed using Sentinel-2 high-resolution spatial images and combined with the Otsu algorithm to automatically retrieve mangrove information. Mangrove vegetation indices were composed using red, green, red-edge, and SWIR1 bands, which enhanced the differences in greenness and moisture characteristics between mangrove and other vegetation, and fully highlighted the information with respect to mangrove. The mangrove on Hainan Island were mapped using this method with an OA of 95.68% and a kappa coefficient of 0.92, and the UA and PA of the mangrove reached 93.68% and 91.26%, respectively.

The new mangrove vegetation index was constructed and combined with the Otsu algorithm to extract mangrove information from Hainan Island, taking into full consideration the limitation of remote sensing data source resolution on feature identification, the shortcomings of the existing mangrove indices in practical applications, and the influence of tides on mangrove identification. The construction of this mangrove vegetation index was based on the spectral characteristics of mangrove, which may be theoretically applicable to the identification and monitoring of mangrove worldwide. Compared with the tedious sample selection and classifier determination required by machine learning, the REMI-based mangrove classification method has more potential with respect to large areas.

## REFERENCES

- [1] C. Zhao, M. Jia, Z. Wang, D. Mao, and Y. Wang, "Identifying mangroves through knowledge extracted from trained random forest models: An interpretable mangrove mapping approach (IMMA)," *ISPRS J. Photogramm. Remote Sens.*, vol. 201, pp. 209–225, Jul. 2023, doi: 10.1016/j.isprsjprs.2023.05.025.

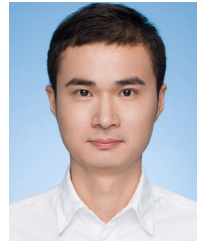
- [2] X. Wang et al., "Tracking annual changes of coastal tidal flats in China during 1986–2016 through analyses of Landsat images with Google Earth Engine," *Remote Sens. Environ.*, vol. 238, Mar. 2020, Art. no. 110987, doi: [10.1016/j.rse.2018.11.030](https://doi.org/10.1016/j.rse.2018.11.030).
- [3] X. Chen, L. Li, and J. Du, "Porewater exchange and the related carbon sink potential in mangroves and saltmarshes," *Adv. Earth Sci.*, vol. 37, no. 9, pp. 881–898, 2022, doi: [10.11867/j.issn.1001-8166.2022.006](https://doi.org/10.11867/j.issn.1001-8166.2022.006).
- [4] L. A. Deegan, J. E. Hughes, and R. A. Rountree, "Salt Marsh ecosystem support of marine transient species," in *Concepts and Controversies in Tidal Marsh Ecology*, M. P. Weinstein and D. A. Kreeger, Eds. Dordrecht, The Netherlands: Kluwer Academic, 2000, pp. 333–365, doi: [10.1007/0-306-47534-0\\_16](https://doi.org/10.1007/0-306-47534-0_16).
- [5] H. V. Habi and H. Messer, "Recurrent neural network for rain estimation using commercial microwave links," *IEEE Trans. Geosci. Remote Sens.*, vol. 59, no. 5, pp. 3672–3681, May 2021, doi: [10.1109/TGRS.2020.3010305](https://doi.org/10.1109/TGRS.2020.3010305).
- [6] W. Sun et al., "A simple and effective spectral-spatial method for mapping large-scale coastal wetlands using China ZY1-02D satellite hyperspectral images," *Int. J. Appl. Earth Observ. Geoinf.*, vol. 104, Dec. 2021, Art. no. 102572.
- [7] D. Mao et al., "Conversions between natural wetlands and farmland in China: A multiscale geospatial analysis," *Sci. Total Environ.*, vol. 634, pp. 550–560, Sep. 2018, doi: [10.1016/j.scitotenv.2018.04.009](https://doi.org/10.1016/j.scitotenv.2018.04.009).
- [8] D. Wang et al., "Estimating aboveground biomass of the mangrove forests on Northeast Hainan Island in China using an upscaling method from field plots, UAV-LiDAR data and Sentinel-2 imagery," *Int. J. Appl. Earth Observ. Geoinf.*, vol. 85, Mar. 2020, Art. no. 101986, doi: [10.1016/j.jag.2019.101986](https://doi.org/10.1016/j.jag.2019.101986).
- [9] A. B. Baloloy, A. C. Blanco, R. R. C. Sta. Ana, and K. Nadaoka, "Development and application of a new Mangrove Vegetation Index (MVI) for rapid and accurate mangrove mapping," *ISPRS J. Photogramm. Remote Sens.*, vol. 166, pp. 95–117, Aug. 2020, doi: [10.1016/j.isprsjprs.2020.06.001](https://doi.org/10.1016/j.isprsjprs.2020.06.001).
- [10] M. Jia, Z. Wang, Y. Zhang, D. Mao, and C. Wang, "Monitoring loss and recovery of mangrove forests during 42 years: The achievements of mangrove conservation in China," *Int. J. Appl. Earth Observ. Geoinf.*, vol. 73, pp. 535–545, Dec. 2018, doi: [10.1016/j.jag.2018.07.025](https://doi.org/10.1016/j.jag.2018.07.025).
- [11] L. Lymburner et al., "Mapping the multi-decadal mangrove dynamics of the Australian coastline," *Remote Sens. Environ.*, vol. 238, Mar. 2020, Art. no. 111185, doi: [10.1016/j.rse.2019.05.004](https://doi.org/10.1016/j.rse.2019.05.004).
- [12] K. Kathiresan and B. L. Bingham, "Biology of mangroves and mangrove ecosystems," *Adv. Mar. Biol.*, vol. 40, pp. 81–251, Dec. 2001, doi: [10.1016/S0065-2881\(01\)40003-4](https://doi.org/10.1016/S0065-2881(01)40003-4).
- [13] N. Thomas, R. Lucas, P. Bunting, A. Hardy, A. Rosenqvist, and M. Simard, "Distribution and drivers of global mangrove forest change, 1996–2010," *PLoS One*, vol. 12, no. 6, Jun. 2017, Art. no. e0179302, doi: [10.1371/journal.pone.0179302](https://doi.org/10.1371/journal.pone.0179302).
- [14] S. K. Marx, J. M. Knight, P. G. Dwyer, D. P. Child, M. A. C. Hotchkiss, and A. Zawadzki, "Examining the response of an Eastern Australian mangrove forest to changes in hydro-period over the last century," *Estuarine, Coastal Shelf Sci.*, vol. 241, Aug. 2020, Art. no. 106813, doi: [10.1016/j.ecss.2020.106813](https://doi.org/10.1016/j.ecss.2020.106813).
- [15] C. Giri, B. Pengra, J. Long, and T. R. Loveland, "Next generation of global land cover characterization, mapping, and monitoring," *Int. J. Appl. Earth Observ. Geoinf.*, vol. 25, pp. 30–37, Dec. 2013, doi: [10.1016/j.jag.2013.03.005](https://doi.org/10.1016/j.jag.2013.03.005).
- [16] C. Chen et al., "Temporal and spatial variation of coastline using remote sensing images for Zhoushan archipelago, China," *Int. J. Appl. Earth Observ. Geoinf.*, vol. 107, Mar. 2022, Art. no. 102711.
- [17] J. Montgomery, C. Mahoney, B. Brisco, L. Boychuk, D. Cobbaert, and C. Hopkinson, "Remote sensing of wetlands in the Prairie pothole region of North America," *Remote Sens.*, vol. 13, no. 19, p. 3878, Sep. 2021, doi: [10.3390/rs13193878](https://doi.org/10.3390/rs13193878).
- [18] C. Zhao, M. Jia, Z. Wang, D. Mao, and Y. Wang, "Toward a better understanding of coastal salt Marsh mapping: A case from China using dual-temporal images," *Remote Sens. Environ.*, vol. 295, Sep. 2023, Art. no. 113664, doi: [10.1016/j.rse.2023.113664](https://doi.org/10.1016/j.rse.2023.113664).
- [19] C. Wang et al., "A snow-free vegetation index for improved monitoring of vegetation spring green-up date in deciduous ecosystems," *Remote Sens. Environ.*, vol. 196, pp. 1–12, Jul. 2017, doi: [10.1016/j.rse.2017.04.031](https://doi.org/10.1016/j.rse.2017.04.031).
- [20] M. K. Ghosh, L. Kumar, and C. Roy, "Mapping long-term changes in mangrove species composition and distribution in the Sundarbans," *Forests*, vol. 7, no. 12, p. 305, Dec. 2016, doi: [10.3390/f7120305](https://doi.org/10.3390/f7120305).
- [21] C. Giri et al., "Distribution and dynamics of mangrove forests of South Asia," *J. Environ. Manage.*, vol. 148, pp. 101–111, Jan. 2015, doi: [10.1016/j.jenvman.2014.01.020](https://doi.org/10.1016/j.jenvman.2014.01.020).
- [22] C. Suwanprasit, "Effects of near shore land-use dynamic on coastal erosion in Phuket, Thailand," in *Proc. IEEE Int. Geosci. Remote Sens. Symp. (IGARSS)*, Jul. 2015, pp. 4832–4835, doi: [10.1109/IGARSS.2015.7326912](https://doi.org/10.1109/IGARSS.2015.7326912).
- [23] T. Wang, H. Zhang, H. Lin, and C. Fang, "Textural-spectral feature-based species classification of mangroves in Mai Po Nature Reserve from Worldview-3 imagery," *Remote Sens.*, vol. 8, no. 1, p. 24, Dec. 2015, doi: [10.3390/rs8010024](https://doi.org/10.3390/rs8010024).
- [24] V. Otero, K. Quisthoudt, N. Koedam, and F. Dahdouh-Guebas, "Mangroves at their limits: Detection and area estimation of mangroves along the Sahara desert coast," *Remote Sens.*, vol. 8, no. 6, pp. 512–520, Jun. 2016, doi: [10.3390/rs8060512](https://doi.org/10.3390/rs8060512).
- [25] J. E. Cubillas and M. Japitana, "The application of support vector machine (SVM) using CIELAB color model, color intensity and color constancy as features for ortho image classification of benthic habitats in Hinatuan, Surigao Del Sur, Philippines," *Int. Arch. Photogramm., Remote Sens. Spatial Inf. Sci.*, vol. 7, pp. 189–194, Jun. 2016, doi: [10.5194/isprs-archives-XLI-B7-189-2016](https://doi.org/10.5194/isprs-archives-XLI-B7-189-2016).
- [26] D. Sikdar, A. Banerjee, P. Das, and S. Datta, "Biodegradation of acenaphthene using two different isolated bacteria: Comparative analysis and optimization using artificial neural network," *Environ. Pollut. Protection*, vol. 1, no. 1, pp. 12–22, Sep. 2016, doi: [10.22606/epp.2016.11002](https://doi.org/10.22606/epp.2016.11002).
- [27] L. Hu, W. Li, and B. Xu, "Monitoring mangrove forest change in China from 1990 to 2015 using Landsat-derived spectral-temporal variability metrics," *Int. J. Appl. Earth Observ. Geoinf.*, vol. 73, pp. 88–98, Dec. 2018, doi: [10.1016/j.jag.2018.04.001](https://doi.org/10.1016/j.jag.2018.04.001).
- [28] K. Kanniah et al., "Satellite images for monitoring mangrove cover changes in a fast growing economic region in Southern Peninsular Malaysia," *Remote Sens.*, vol. 7, no. 11, pp. 14360–14385, Oct. 2015, doi: [10.3390/rs71114360](https://doi.org/10.3390/rs71114360).
- [29] J. Zhen, J. Liao, and G. Shen, "Remote sensing monitoring and analysis on the dynamics of mangrove forests in Qinglan Harbor of Hainan Province since 1987," *Wetland Sci.*, vol. 17, no. 1, pp. 44–51, Feb. 2019, doi: [10.13248/j.cnki.wetlandsci.2019.01.006](https://doi.org/10.13248/j.cnki.wetlandsci.2019.01.006).
- [30] L. Ma, M. Li, X. Ma, L. Cheng, P. Du, and Y. Liu, "A review of supervised object-based land-cover image classification," *ISPRS J. Photogramm. Remote Sens.*, vol. 130, pp. 277–293, Aug. 2017, doi: [10.1016/j.isprsjprs.2017.06.001](https://doi.org/10.1016/j.isprsjprs.2017.06.001).
- [31] A. R. Huete, K. Didan, T. Miura, E. P. Rodriguez, X. Gao, and L. G. Ferreira, "Overview of the radiometric and biophysical performance of the MODIS vegetation indices," *Remote Sens. Environ.*, vol. 83, nos. 1–2, pp. 195–213, 2002, doi: [10.1016/S0034-4257\(02\)00096-2](https://doi.org/10.1016/S0034-4257(02)00096-2).
- [32] B. Matsushita, W. Yang, J. Chen, Y. Onda, and G. Qiu, "Sensitivity of the Enhanced Vegetation Index (EVI) and Normalized Difference Vegetation Index (NDVI) to topographic effects: A case study in high-density cypress forest," *Sensors*, vol. 7, no. 11, pp. 2636–2651, Nov. 2007, doi: [10.3390/s7112636](https://doi.org/10.3390/s7112636).
- [33] G. Winarso, A. D. Purwanto, and D. Yuwono, "New mangrove index as degradation/health indicator using remote sensing data: Segara Anakan and Alas Purwo case study," in *Proc. 12th Biennial Conf. Pan Ocean Remote Sens.*, 2014, pp. 4–7.
- [34] T. Shi, J. Liu, Z. Hu, H. Liu, J. Wang, and G. Wu, "New spectral metrics for mangrove forest identification," *Remote Sens. Lett.*, vol. 7, no. 9, pp. 885–894, Sep. 2016, doi: [10.1080/2150704X.2016.1195935](https://doi.org/10.1080/2150704X.2016.1195935).
- [35] X. Zhang and Q. Tian, "A mangrove recognition index for remote sensing of mangrove forest from space," *Current Sci.*, vol. 105, no. 8, pp. 1149–1154, Oct. 2013, doi: [10.3186/jjphytopath.71.326](https://doi.org/10.3186/jjphytopath.71.326).
- [36] K. Gupta et al., "An Index for discrimination of mangroves from non-mangroves using LANDSAT 8 OLI imagery," *MethodsX*, vol. 5, pp. 1129–1139, Sep. 2018, doi: [10.1016/j.mex.2018.09.011](https://doi.org/10.1016/j.mex.2018.09.011).
- [37] M. Jia, Z. Wang, C. Wang, D. Mao, and Y. Zhang, "A new vegetation index to detect periodically submerged mangrove forest using single-tide Sentinel-2 imagery," *Remote Sens.*, vol. 11, no. 17, p. 2043, Aug. 2019, doi: [10.3390/rs11172043](https://doi.org/10.3390/rs11172043).
- [38] M. Jia et al., "Mapping global distribution of mangrove forests at 10-m resolution," *Sci. Bull.*, vol. 68, no. 12, pp. 1306–1316, Jun. 2023, doi: [10.1016/j.scib.2023.05.004](https://doi.org/10.1016/j.scib.2023.05.004).
- [39] J. Liao, B. Zhu, Y. Chang, and L. Zhang, "A dataset of mangrove forest changes on Hainan Island based on GF-2 data during 2015–2019," *China Sci. Data*, vol. 7, no. 4, pp. 1–11, Dec. 2022, doi: [10.11922/11-6035.noda.2021.0016.zh](https://doi.org/10.11922/11-6035.noda.2021.0016.zh).

- [40] C. Fang, L. Wang, and H. Xu, "A comparative study of different red edge indices for remote sensing detection of urban grassland health status," *J. Geo-Inf. Sci.*, vol. 19, no. 10, pp. 1382–1392, 2017, doi: [10.3724/SP.J.1047.2017.01382](https://doi.org/10.3724/SP.J.1047.2017.01382).
- [41] D. Wang et al., "Evaluating the performance of Sentinel-2, Landsat 8 and Pléiades-1 in mapping mangrove extent and species," *Remote Sens.*, vol. 10, no. 9, p. 1468, Sep. 2018, doi: [10.3390/rs10091468](https://doi.org/10.3390/rs10091468).
- [42] C. Schuster, M. Förster, and B. Kleinschmit, "Testing the red edge channel for improving land-use classifications based on high-resolution multi-spectral satellite data," *Int. J. Remote Sens.*, vol. 33, no. 17, pp. 5583–5599, Sep. 2012, doi: [10.1080/01431161.2012.666812](https://doi.org/10.1080/01431161.2012.666812).
- [43] T. Kumar, A. Mandal, D. Dutta, R. Nagaraja, and V. K. Dadhwal, "Discrimination and classification of mangrove forests using EO-1 Hyperion data: A case study of Indian Sundarbans," *Geocarto Int.*, vol. 34, no. 4, pp. 415–442, Mar. 2019, doi: [10.1080/10106049.2017.1408699](https://doi.org/10.1080/10106049.2017.1408699).
- [44] I. Herrmann, A. Karnieli, D. J. Bonfil, Y. Cohen, and V. Alchanatis, "SWIR-based spectral indices for assessing nitrogen content in potato fields," *Int. J. Remote Sens.*, vol. 31, no. 19, pp. 5127–5143, Oct. 2010, doi: [10.1080/01431160903283892](https://doi.org/10.1080/01431160903283892).
- [45] K. A. Prasad and L. Gnanappazham, "Multiple statistical approaches for the discrimination of mangrove species of *Rhizophoraceae* using transformed field and laboratory hyperspectral data," *Geocarto Int.*, vol. 31, no. 8, pp. 891–912, Oct. 2015, doi: [10.1080/10106049.2015.1094521](https://doi.org/10.1080/10106049.2015.1094521).
- [46] S. Seager, E. L. Turner, J. Schafer, and E. B. Ford, "Vegetation's red edge: A possible spectroscopic biosignature of extraterrestrial plants," *Astrobiology*, vol. 5, no. 3, pp. 372–390, Jun. 2005, doi: [10.1089/ast.2005.5.372](https://doi.org/10.1089/ast.2005.5.372).
- [47] Y. Kanke, B. Tubaña, M. Dalen, and D. Harrell, "Evaluation of red and red-edge reflectance-based vegetation indices for rice biomass and grain yield prediction models in paddy fields," *Precis. Agricult.*, vol. 17, no. 5, pp. 507–530, Oct. 2016, doi: [10.1007/s11119-016-9433-1](https://doi.org/10.1007/s11119-016-9433-1).
- [48] M. Jia, Z. Wang, D. Mao, C. Ren, C. Wang, and Y. Wang, "Rapid, robust, and automated mapping of tidal flats in China using time series Sentinel-2 images and Google Earth Engine," *Remote Sens. Environ.*, vol. 255, Mar. 2021, Art. no. 112285, doi: [10.1016/j.rse.2021.112285](https://doi.org/10.1016/j.rse.2021.112285).
- [49] Q. Han and Z. Niu, "China intertidal zone dataset based on tidal correction," *J. Glob. Change Data Discovery*, vol. 3, no. 1, pp. 42–47, Jan. 2019, doi: [10.3974/geodp.2019.01.06](https://doi.org/10.3974/geodp.2019.01.06).



**Zhaojun Chen** is currently pursuing the master's degree in forestry with the Central South University of Forestry and Technology, Changsha, China.

Her major research interests include resources and environmental remote sensing and GIS.



**Meng Zhang** received the M.S. degree in geography from Hunan Normal University, Changsha, China, in 2014, and the Ph.D. degree in cartography and geographic information engineering from Central South University, Changsha, in 2018.

He is currently a Teacher with the College of Forestry, Central South University of Forestry and Technology, Changsha. He has authored more than 40 research articles indexed by SCI and Engineering Index (EI). His research interests include resources and environmental remote sensing and GIS.



**Huaiqing Zhang** received the M.S. and Ph.D. degrees in forest management from the Chinese Academy of Forestry (CAF), Beijing, China, in 1998 and 2001, respectively.

He is currently a Professor, a Chief Expert on visualization and simulation, and the Director of the Department of Visualization Simulation and Monitoring, Institute of Forest Resources Information Techniques, Chinese Academy of Forestry. His major research interests include forest visualization and simulation techniques, and monitoring of wetland resources using satellite and ground-based sensors.



**Yang Liu** received the B.S. degree in digital media technology from Harbin Normal University, Harbin, China, in 2017. She is currently pursuing the master's degree with the Institute of Forest Resources Information Techniques, Chinese Academy of Forestry, Beijing, China.

Her major research interests include satellite and ground-based sensors for wetland resource monitoring.